A&A 620, A193 (2018)
https://doi.org/10.1051/0004-6361/201732495

Astronomy & Astrophysics

The VIMOS Public Extragalactic Redshift Survey (VIPERS)

AGN feedback in [NeV] emitters⋆

D. Vergani[1], B. Garilli[2], M. Polletta[2,3,4], P. Franzetti[2], M. Scodeggio[2], G. Zamorani[1], C. P. Haines[5], M. Bolzonella[1], L. Guzzo[5,6], B. R. Granett[5,6], S. de la Torre[7], U. Abbas[8], C. Adami[7], D. Bottini[2], A. Cappi[1,9], O. Cucciati[1,10], I. Davidzon[7,1], G. De Lucia[11], A. Fritz[2], A. Gargiulo[2], A. J. Hawken[5,6], A. Iovino[5], J. Krywult[12], V. Le Brun[7], O. Le Fèvre[7], D. Maccagni[2], K. Małek[13], F. Marulli[10,14,1], A. Pollo[13,15], L. A. M. Tasca[7], R. Tojeiro[16], A. Zanichelli[17], S. Arnouts[7], J. Bel[18], E. Branchini[19,20,21], J. Coupon[22], O. Ilbert[7], and T. Moutard[23,7], and L. Moscardini[10,14,1]

(Affiliations can be found after the references)

Received 19 December 2017 / Accepted 18 October 2018

ABSTRACT

Aims. We analyse the properties of the host galaxies of a [NeV]-selected sample to investigate whether and how they are affected by the AGN.
Methods. We have selected a sample of galaxies at $0.62 < z < 1.2$ from the VIMOS Public Extragalactic Redshift Survey (VIPERS) and divided it in blue cloud galaxies, red passive galaxies and green valley galaxies using the NUVrK diagram. Within each category, galaxies with AGN activity were identified based on the detection of the high-ionisation [NeV]λ3426 emission line. For each galaxy we derived several properties (stellar age and mass, the $(r-K)$ colour, the [OII] luminosity) and compared them between active and inactive galaxies matched in stellar mass and redshift.
Results. We find statistically significant differences in the properties between active and inactive galaxies. These differences imply that the AGN is more often found in galaxies with younger stellar populations and more recent star-forming activity than their parent samples. Interestingly, the AGN identified through the [NeV]λ3426 emission line is not commonly found by traditional AGN-selection techniques based on shallow X-ray data, mid-IR colours, and classical line diagnostic diagrams, and might thus reveal a specific evolutionary phase. The spectral analysis reveals a sub-set of AGN within the blue cloud that has spectral signatures implying a sudden suppression of star formation activity similar to post-starburst galaxies.
Conclusion. Using the rich dataset of the large VIPERS sample we identify a novel class of active post-starburst galaxies that would be missed by traditional selection techniques. These galaxies belong to the blue cloud, but their star-formation activity has been recently suppressed, possibly by the AGN identified through the presence of the [NeV]λ3426 emission line in their spectra. Our results support the idea that AGN feedback may be responsible for halting star-formation in active blue galaxies and for their transition into the red sequence, at least in the 0.6−1.2 redshift range and for stellar masses greater than $5 \times 10^{10}\,\mathcal{M}_{\odot}$. Our results are based on a complete spectroscopic sample and limited by the [NeV] observability, and the AGN can be variable and with a relatively short duty cycle. Considering this, AGN feedback that makes blue galaxies quickly transition to the red sequence may be even more common than previously believed.

Key words. galaxies: active – galaxies: evolution – galaxies: star formation – cosmology: observations

1. Introduction

Various mechanisms have been proposed to explain the ceasing of star formation activity in galaxies. They are cluster-related mechanisms, such as ram-pressure gas stripping, harassment, or strangulation (Gunn & Gott 1972; Larson et al. 1980; Balogh & Morris 2000), including events such as galaxy mergers and interactions (Toomre & Toomre 1972; Barnes & Hernquist 1992), commonly found in both the field and in clusters (although more efficient in the field). Energetic feedback from active galactic nuclei and supernovae (AGN/SN) also contributes to star formation quenching (Springel et al. 2005; Hopkins et al. 2007), but how much and in which ways is still a matter of debate. These processes should be more or less efficient at different mass scales (Kaviraj et al. 2007). While AGN feedback is intriguing because it can justify several relationships between the properties of the central supermassive black holes and their host properties, finding evidence of star formation quenching by AGN activity is challenging and it is not clear whether it is an efficient and ubiquitous process.

The first complexity in investigating this topic is related to the collection of a reliable sample of sources that host AGNs. The presence of an AGN can be found through several signatures, which are not always ubiquitous. Different selection techniques target specific properties and yield different identification rates; completeness and reliability are often complementary. The selection biases need to be taken into account to be able to evaluate the role of the AGN and whether it has an impact on the host galaxy. The most common selection criteria are based on X-ray, mid-infrared, radio, and spectroscopic observations. Deep X-ray surveys have provided the most effective method of identifying reliable and fairly complete samples of AGN out to high

⋆ Based on observations collected at the European Southern Observatory, Cerro Paranal, Chile, using the Very Large Telescope under programmes 182.A-0886 and partly 070.A-9007. Also based on observations obtained with MegaPrime/MegaCam, a joint project of CFHT and CEA/DAPNIA, at the Canada-France-Hawaii Telescope (CFHT), which is operated by the National Research Council (NRC) of Canada, the Institut National des Sciences de l'Univers of the Centre National de la Recherche Scientifique (CNRS) of France, and the University of Hawaii. This work is based in part on data products produced at TERAPIX and the Canadian Astronomy Data Centre as part of the Canada-France-Hawaii Telescope Legacy Survey, a collaborative project of NRC and CNRS. The VIPERS web site is http://www.vipers.inaf.it/

redshifts (e.g. see Brandt & Hasinger 2005, for a review), but they suffer from incompleteness of the most obscured sources when Compton-thick mechanisms are at work (Della Ceca et al. 2008; Comastri et al. 2011; Brightman et al. 2014). Unfortunately Compton-thick AGNs represent a sizable fraction of the full AGN population, of the order of 35% of the entire AGN population at all redshifts (Akylas & Georgantopoulos 2009; Vignali et al. 2010; Alexander et al. 2011; Buchner et al. 2015). Other techniques that provide reliable AGN samples are based on the radio emission or on the width and strength of emission lines. Radio selection techniques have traditionally been applied to identify radio-loud AGN, where the radio emission is mainly powered by the AGN. This class of AGN, representing about 10% of the whole AGN population, is identified through high observed radio powers (Zamfir et al. 2008), an excess of radio emission beyond what is expected from star formation (Wilkes & Elvis 1987; Kellermann et al. 1989; Appleton et al. 2004), or the shape of the radio spectrum (Morganti 2017; and references therein). The radio-based selection methods yield reliable AGN samples, but they represent a minority of the full AGN population and are biased toward a certain type of AGN or evolutionary phase. Plus care must be taken when applying the radio selection at $z > 0.1$ as the selection criteria depend on the redshift. Diagnostics based on emission line ratios evaluating the excitation mechanisms of the emitting gas have been used in low-z optical surveys (Baldwin et al. 1981). At intermediate redshifts the diagnostics based on the mass excitation (MEx) and the colour excitation efficiently separate AGNs, star forming, and composite galaxies (Juneau et al. 2011, 2014; Yan et al. 2011). Other approaches using a combination of different spectral features have been used at higher-z (e.g. the [OII] and Hβ vs. [OIII]/Hβ by Lamareille 2010). However, they all mandate a full coverage of the spectral window from [OII] up to [OIII], thus limiting the selection to a small redshift range.

Other complexities arising in the study of star formation quenching by AGN activity include the size and the nature of the galaxy samples. Investigations of AGN feedback are often based on transition galaxies. Among them, the most generally used are galaxies in the green valley, which are interpreted to be in a transitioning stage between the blue cloud and the red sequence (Martin et al. 2007). Although independent both on the type of quenching process and on galaxy mass (Trayford et al. 2016), catalogues of green galaxies selected with photometric criteria are normally scanty. The dearth of points in this region of the colour–colour diagram is explained by the short time required by a galaxy to cross the green valley (up to 1−2 Gyr).

If photometric criteria are not producing sizable catalogues of transiting galaxies, those selected spectroscopically suffer from similar complexities. This class of galaxies – dubbed the post-starburst galaxies – exhibit strong Balmer absorption lines and no, or very faint emission lines (Dressler & Gunn 1983). This combination of peculiar spectral features is indicative of a major burst of star formation activity that has recently terminated. Apart from the scarcity of these sources, as pointed out before, there is the need to have sufficient signal-to-noise in the spectra. An incompleteness of recently quenched galaxies with nuclear activity in spectroscopically selected samples has also been noticed. Since the AGN can produce some of the emission lines commonly observed in star forming galaxies (e.g. [OII] line, Kauffmann et al. 2003b; Davies et al. 2014), post-starburst galaxies hosting AGN activity are missed by the standard spectroscopically-based post-starburst selection techniques (Yan et al. 2006). These latter techniques require weak or absent emission lines, that is, an [OII] equivalent width >-2.5 Å or >-4.0 Å (where negative values refer to emission), and Hδ in absorption with EW(Hδ) $> 3.0-4.0$ Å the exact values depending on the authors (e.g. Goto et al. 2003; Vergani et al. 2010).

To overcome the above-mentioned shortcomings we used a photometric criterion to select transition galaxies from the largest spectroscopic survey currently available at intermediate redshifts, the VIMOS Public Extragalactic Redshift Survey, (VIPERS; Guzzo et al. 2014; Garilli et al. 2014; Scodeggio et al. 2018). The spectroscopic data were used to trace AGN activity and investigate whether it plays a role in regulating the star formation activity in the host galaxy by analysing star-formation tracers like the [OII] luminosity, as well as colour, stellar mass and age.

The existence of the [NeV]λ3426 emission line in a galactic spectrum implies the presence of hard radiation with photon energies above 96.6 eV, that is, in the extreme-ultraviolet and soft X-ray range. Other works have used the high-ionisation potential of the [NeV]λ3426 emission line to establish the presence of gas photoionised by an AGN (Feltre et al. 2016; Mignoli et al. 2013). The selection based on the detection of the [NeV] line yields a highly reliable AGN sample (Gilli et al. 2010; Mignoli et al. 2013). In VIPERS it offers a unique opportunity to obtain a large sample of galaxies hosting an AGN activity at optical wavelengths over the nearly entire redshift range covered by this survey.

In this work, we present a sample of 529 galaxies at redshift $0.62 \leq z \leq 1.2$ with the high-ionisation narrow emission line [NeV]λ3426 as a tracer of AGN activity in the VIPERS spectra. These candidates are selected to examine whether the AGN leaves an imprint on the host properties and, in particular, if there is any evidence of quenching that could be attributed to the AGN negative feedback. Out of the scope of this paper is a detailed discussion on the methodologies of selecting AGNs. In addition, we do not include the AGNs for which the star formation is not the predominant source of emission (type 1 AGNs) in our analysis, because their optical spectra is dominated by AGN emission, and so study of the host stellar populations is too uncertain.

This work is organised as follows: the data and sample selection are presented in Sect. 2; results are described in Sect. 3, and a discussion and conclusions are given in Sects. 4 and 5. Throughout this work, we have assumed a standard cosmological model with $\Omega_M = 0.3$, $\Omega_\Lambda = 0.7$, and $H_0 = 70\,\mathrm{km\,s^{-1}\,Mpc^{-1}}$. Magnitudes are given in the AB system.

2. Selection of [NeV] emitters

2.1. General overview of the survey

The VIPERS project is the largest redshift survey to date of galaxies in the redshift range $z = [0.5-1.2]$. Its target galaxies have been selected from the Canada-France-Hawaii Telescope Legacy Survey Wide (CFHTLS-Wide) over the W1 and W4 fields (see Guzzo et al. 2014) and probes a volume of $\sim 1.5 \times 10^8\,\mathrm{Mpc^3\,H_{70}^{-3}}$ for a total of $24\,\mathrm{deg^2}$. The survey is a combination of a flux-limited ($i_{AB} < 22.5$) sample with $(u-g)-(r-i)$ colour selections to focus on galaxies at intermediate redshifts and comprises about 100 000 redshifts.

The VIPERS objects are observed with the red $R \sim 210$ VIMOS LR grism covering the spectral range 5500–9500 Å. All details of the observations and data handling are contained in Guzzo et al. (2014), and Garilli et al. (2012, 2014), which also describe other important aspects of this survey. In particular, we have adopted the observing strategy proposed by Scodeggio et al. (2009) to maximise the number of objects to

be observed in a single pass using minimal slit length. Thanks to this choice the target sampling rate (the ratio of observed targets over the total number of targets) is ∼45%. In this work, we have used the 76 552 galaxies of the final VIPERS data release with highly reliable spectroscopic redshifts, in other words, those objects with $z_{\rm flag} = [2-4]$ that have an average confidence level larger than 96% to be correct (Scodeggio et al. 2018; Guzzo et al. 2014). We describe the other relevant quantities used in this work, such as the stellar mass, magnitudes, and line fluxes in Sects. 2.2 and 2.3, and we refer the reader to the following papers for fully explained details (Guzzo et al. 2014; Garilli et al. 2014; Scodeggio et al. 2018; Moutard et al. 2016a,b; Davidzon et al. 2013, 2016).

2.2. [NeV] emitters and their parent galaxies in the NUVrK diagram

We use the rest-frame (NUV−r) vs. (r−K) diagram, or NUVrK diagram (Fig. 1) to select our sample of green galaxies and the corresponding control samples of red and blue galaxies (Ilbert et al. 2013; Davidzon et al. 2016). The NUVrK diagram provides more reliable classifications than other galaxy classifying techniques, as for example single colour classifications or the UVJ diagram (Williams et al. 2009). Its main advantage is the capability of effectively separating the influence of dust extinction and ageing of the stellar populations (see e.g. Moutard et al. 2016a,b). We defined the green valley as the locus satisfying the following colour criteria:

$$\begin{aligned}&\text{for } (r-K) \leq 0.4\\ &\quad 3.13 < (\mathrm{NUV} - r) < 3.73\\ &\text{for } 0.4 < (r-K) < 1.35\\ &\quad 1.37 \times (r-K) + 2.6 < (\mathrm{NUV} - r) < 1.37 \times (r-K) + 3.18\end{aligned} \tag{1}$$

by using absolute magnitudes and stellar masses following the methodology used in Moutard et al. (2016b). To account for colour uncertainties we exclude a region of 0.25 mag around the green valley locus.

The galaxies in the NUVrK diagram above and below the extended green valley region, defined as in Eq. (1) and then expanded in all directions by 0.25 mag (grey solid lines in Fig. 1), represent the comparison samples of the red (quiescent) and blue (star-forming) galaxies, respectively. We have used the high-ionisation potential of the [NeV]λ3426 emission line to reveal the presence of gas photoionisation by AGN (Schmidt et al. 1998; Gilli et al. 2010; Mignoli et al. 2013; Feltre et al. 2016). We define the [NeV] emitters as galaxies that show a [NeV]λ3426 line satisfying the following conditions:

1. The FWHM of the line is between 7 Å and 22 Å this is equivalent to requiring the full line width to be from one to three resolution elements given the resolution of VIPERS spectra. These values have been defined based on several tests carried out on the main emission lines observed in the VIPERS spectra, a random sub-sample of which were visually inspected.
2. The line flux is detected at ≥2σ. Here the flux is computed as the integral of the Gaussian best fit to the emission line, and the error on the flux takes into account the error on the continuum, the Poissonian error on line counts, and the Gaussian fit residuals.

When the line is not detected, we have computed the upper limit to the flux as 3 times the rms noise of the continuum adjacent to the [NeV]λ3426 line. Considering both detections and upper limits, our sample is representative of [NeV]λ3426 emitters having line luminosities larger than 2.1×10^{40} erg s^{-1} with median equivalent width for the [NeV] line of about 7 Å over the redshift interval $z = [0.62-1.20]$.

2.3. Selection of representative catalogues

As all other flux-limited surveys, VIPERS suffers from the classical selection biases induced by the flux limit selection. The common methodology to overcome this kind of selection bias is to impose a luminosity or mass cut, deriving luminosity or mass complete samples. Within VIPERS, the stellar mass completeness limit is $\log(\mathcal{M}_*/\mathcal{M}_\odot) = 10.89$ over the redshift interval $z = [0.62-0.90]$ and $\log(\mathcal{M}_*/\mathcal{M}_\odot) = 11.20$ above redshift $z = 0.9$ (Cucciati et al. 2017). Applying the mass completeness cut at $z = [0.62-0.90]$, our sample would be composed of 1435, 719, and 528 galaxies in the red, green, and blue regions, respectively. Unfortunately, with such a drastic cut the number of [NeV]λ3426 emitters becomes very low, leaving only 32, 17, and 41 galaxies in the three colour classes. Reducing the redshift interval down to $z = [0.62-0.80]$, and thus lowering the stellar mass completeness limit to $\log(\mathcal{M}_*/\mathcal{M}_\odot) = 10.66$, the number of [NeV]$\lambda$3426 emitters remains at a similar low level.

In order to have a robust, and reasonably large catalogue of [NeV]λ3426 emitting galaxies that is not hampered by selection biases due to the survey flux limit selection criterion and still suitable for properly comparing the properties of these [NeV] emitting galaxies with those of the parent samples of non-[NeV] emitters, we have adopted the matching technique on both redshift and stellar mass. With this methodology, we were able to obtain sub-samples of galaxies with equivalent distributions of stellar mass and redshift, while spanning a wider interval of galaxy properties compared to the adoption of a pure stellar mass completeness criterion. The procedure firstly divides the samples of red, green, and blue galaxies defined in Eq. (1). into cells defined in the stellar mass vs. redshift plane. As we are interested in the green galaxies, we take them as reference sample. For each reference cell 0.25 dex wide in stellar mass and 0.20 in redshift, we extracted sub-samples of red and blue galaxies that match the stellar mass and redshift distributions of the green galaxies in the corresponding cells. Thanks to the dimensions of the VIPERS survey, we can afford to double the size of the red and blue galaxy sub-samples in each cell with respect to that of the green galaxies. The total number of objects in the matched stellar mass−redshift sub-samples is 2636 green galaxies and 5272 galaxies in each of the red and blue catalogues, covering the redshift range $z = [0.62-1.20]$.

We repeated the matching algorithm so as to have 20 sub-samples of galaxies with equivalent stellar mass and redshift distributions for the comparison populations of the red and blue galaxies. We used these 20 sub-samples to evaluate the robustness of the results for the red and blue samples. In all of the following figures, we plot the median values of the properties of these sub-samples, while the error bars are the median absolute deviations. For the green galaxies, which are our reference sample and for which we cannot use the multiple catalogues extraction method, the quoted error are Poissonian errors. Finally, from each matched sample we extract the sub-sample of [NeV] emitters, which are the subject of our investigation. The matched samples contain 95 ± 9 (3.6%) green [NeV] emitters, 158 ± 2.5 (3.0%) red ones, and 276 ± 11 (5.2%) blue ones. Using the mean instead of the median, the number of blue and red [NeV] emitters does not change significantly.

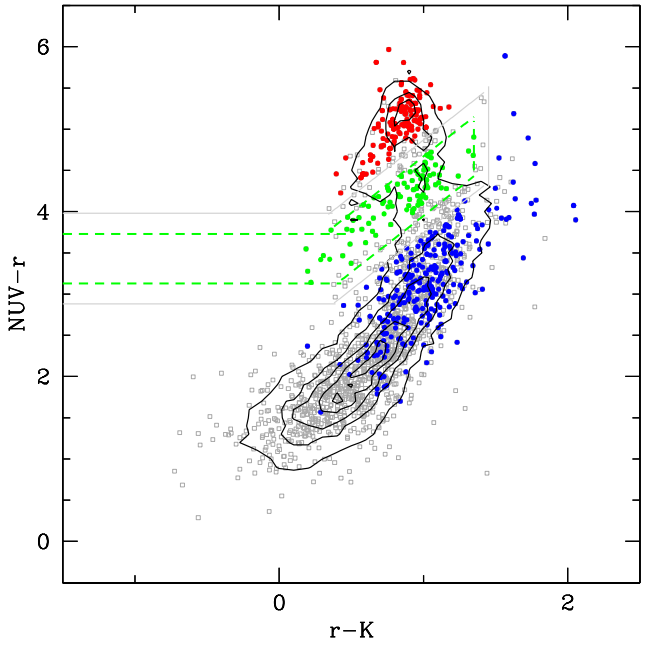

Fig. 1. Rest-frame (NUV−r) vs. ($r-K$) colours for VIPERS galaxies at z = [0.62−1.2]. Isophotal contours outline the loci of the whole VIPERS flux limited sample (contours are in steps of 10% with the faintest isophote level starting at the 10% level). The grey open circles represent all [NeV]λ3426 emitters in the flux-limited catalogue. The dashed green lines show the region of the green valley as defined in Eq. (1). This is surrounded by a 0.25 mag wide region which we have excluded to account for colour uncertainties. The comparison samples of the red and blue galaxies occupy the regions above and below the solid grey line, respectively. The filled circles – colour coded according to their classes, show the [NeV]λ3426 emitters extracted from the stellar mass−redshift matched sub-samples.

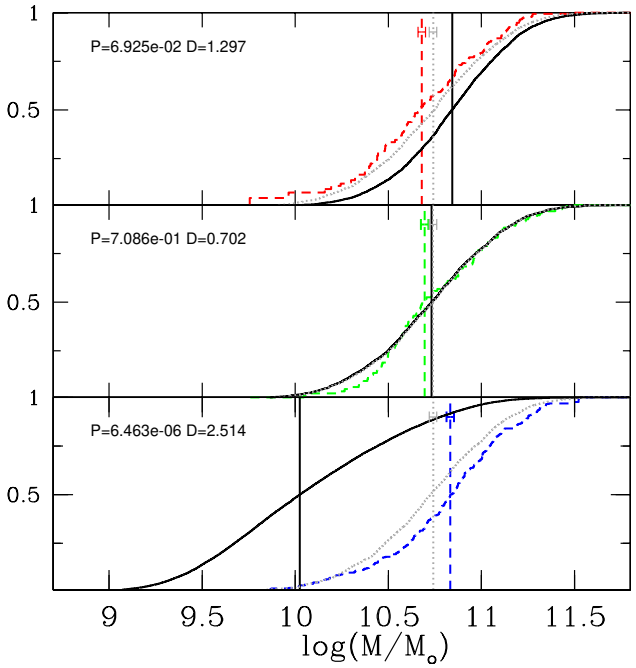

Fig. 2. Stellar mass cumulative distributions in the matched samples (dotted grey curves) for the red, green, and blue galaxies *from top to bottom*. The stellar mass distributions in the flux-limited samples (solid black curves) and that of the [NeV] emitters (extracted from the matched samples and shown with dashed curves, colour-coded accordingly) are also shown together with their median values (vertical lines and same style as before). The error bars plotted at the top of the vertical lines represent the median standard deviation of parent and [NeV] distributions. The Kolmogorov–Smirnov test (probability and distance quoted in each panel) confirms as statistically significant the difference between stellar mass distributions of [NeV] emitters and their parent matched samples in the blue cloud (but not in the green and red subsamples). The blue [NeV] emitters are significantly more massive than the red [NeV] emitters (cf. dashed curves in the *top* and *bottom panels*).

The sub-samples of [NeV] emitters in the matched catalogues are plotted in Fig. 1 with symbols colour coded according to their colour-selected classes. For each visualisation in this work, we have chosen the sample among the 20 sub-samples that shows properties closest to the median properties of the 20 multiple extraction sub-samples.

The strategy of the VIPERS survey was to spectroscopically observe only a fraction of objects in the field of view (45%, see Sect. 2.1). Statistical weights can be applied to make this sample representative of the whole galaxy population (e.g. Davidzon et al. 2013). They take into account the fraction of photometric objects that have been actually targeted and the fraction of them with a secure identification. We note that our selection does not suffer of incompleteness due to the colour cuts applied in selecting VIPERS targets, as this affects only galaxies at $z < 0.6$ (Cucciati et al. 2017). In the analysis of the various derived parameters described below, we verified that the results do not change when correcting for non-targeted and unidentified sources. This indicates that the selected VIPERS sample is representative of the parent photometric sample.

3. Analysis and results

To obtain a coherent picture of the nature of the selected [NeV]λ3426 emitters in the context of the AGN feedback scenario, we have compared several properties with those of their matched parent samples in the blue cloud, green valley, and red sequence.

3.1. Stellar mass distribution

Figure 2 shows the cumulative distributions of the stellar mass for the red (top), green (middle), and blue galaxies (bottom). The black curves are the mass distributions of the full flux-limited samples, the grey dotted curves are the mass distributions of the stellar mass−redshift matched samples, while the coloured dashed curves are the mass distributions of the [NeV] emitters extracted from the matched samples. The vertical lines represent the median values of the stellar mass distribution of these sub-samples. The stellar mass distributions of the stellar mass−redshift matched samples (dotted grey curves) are equal by construction, the median value being $\log(\mathcal{M}_*/\mathcal{M}_\odot)_{\rm parent} = 10.74 \pm 0.02$.

The mass range covered by the stellar mass−redshift matched samples for the red and the blue galaxies is narrower than the mass range covered by the full flux limited sample of red or blue galaxies. This is intrinsic to the matching technique, which excludes from the matching catalogue objects with stellar masses not represented in all the three colour-selected samples at equivalent redshifts. As a consequence, also the [NeV] emitters with very low or very high mass are excluded from the red and blue matched samples. This is particularly noticeable looking at the [NeV] emitters of the blue cloud in Fig. 1: a long tail of [NeV] emitters with very blue colours that have stellar mass values below the lower mass limit of the stellar mass−redshift

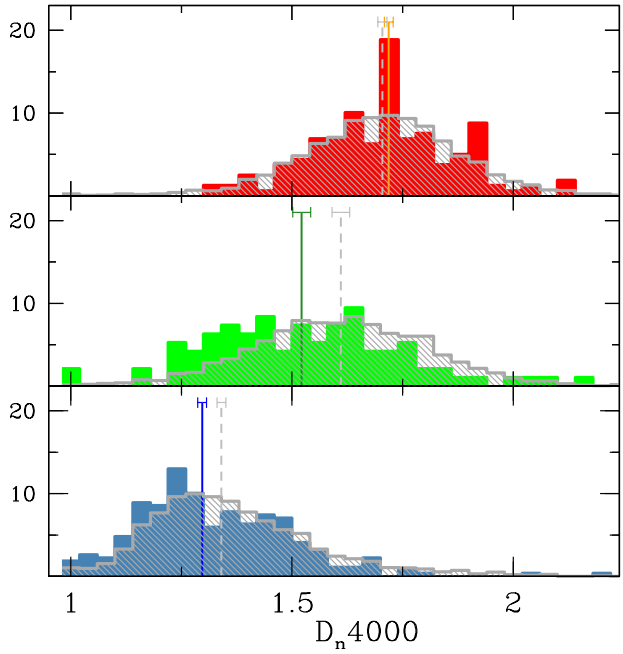

Fig. 3. D_n4000 index distributions for the red, green, and blue [NeV] emitters plotted as filled coloured histograms (*from top to bottom panels*, respectively). The dashed, grey histograms represent the control samples of each population. The median D_n4000 value for each class is overplotted (solid coloured line for the [NeV] emitters and dashed grey line for the comparison samples). The errorbars plotted at the top of the vertical lines represent the median standard deviation of each distribution. The [NeV] emitters of the green valley and those of the blue cloud have younger underlying stellar populations compared to their parent populations.

matched samples are excluded from the analysis (see Fig. 2 bottom panel, solid black vs. dotted grey curves).

We compared the mass distributions of the [NeV] emitters and those of their matched parent samples by applying the Kolmogorov–Smirnov (KS) test. No significant difference is found with the KS-test between the [NeV] emitters and their parent samples in the green and in the red sub-samples, that have differences in their median values never above 3σ level, i.e. $\log(\mathcal{M}_*/\mathcal{M}_\odot)_{\rm red,NeV} = 10.68 \pm 0.02$, and $\log(\mathcal{M}_*/\mathcal{M}_\odot)_{\rm green,NeV} = 10.70 \pm 0.02$ vs. $\log(\mathcal{M}_*/\mathcal{M}_\odot)_{\rm parent} = 10.74 \pm 0.02$ (see the dotted grey vertical lines for the parent sample, and dashed green and red vertical lines for [NeV] emitters in Fig. 2). The test finds instead a statistically significant difference in the stellar mass distributions of the [NeV] emitters in the blue cloud and of their parent matched sample, and this is supported by a 5σ difference in the median stellar mass values (in other words, $\log(\mathcal{M}_*/\mathcal{M}_\odot)_{\rm blue,NeV} = 10.88 \pm 0.02$ vs. $\log(\mathcal{M}_*/\mathcal{M}_\odot)_{\rm parent} = 10.74 \pm 0.02$ (see dashed blue and dotted grey vertical lines in Fig. 2). The blue [NeV] emitters are thus significantly more massive than their parent matched sample, and more massive than the [NeV] emitters in the other sub-samples.

3.2. Stellar ages

The strength of the 4000 Å breaks (D_n4000) can be used as an estimator of the age of stellar populations (e.g. Hamilton 1985), and using the narrow D_n4000 definition (Balogh et al. 1999) further reduces the effect of dust reddening (see for details Kauffmann et al. 2003b). Figure 3 shows the D_n4000 distribution for the [NeV] emitters (coloured filled histograms) and for the stellar mass−redshift matched comparison samples (grey dashed histograms) for the red, green and blue populations. Solid and dashed vertical lines indicate the medians of the different distributions. The errors computed using the resampled catalogues are overplotted. Being systems with absent or negligible star-formation activity, red galaxies have old underlying stellar populations, typically described by large 4000 Å break (e.g. Kauffmann et al. 2003c; Vergani et al. 2008). In our red sample the median value is $D_n4000_{\rm red} = 1.70 \pm 0.01$. On the contrary, galaxies in the blue cloud are actively forming stars and are characterised by low values of the 4000 Å break, $D_n4000_{\rm blue} = 1.34 \pm 0.01$ (see also Haines et al. 2017, for these trends in the VIPERS sample). The green galaxies, consistent with the interpretation of being a population in transition between the blue cloud and the red sequence, show intermediate values of the 4000 Å break, $D_n4000_{\rm green} = 1.61 \pm 0.02$. Interestingly, we find that the blue and green galaxies with nuclear activity traced by [NeV] emission show statistically significantly lower D_n4000 values compared to their parent samples ($D_n4000_{\rm green,neon} = 1.52 \pm 0.02$, $D_n4000_{\rm blue,neon} = 1.30 \pm 0.01$). Instead there is no statistical difference between the red [NeV] emitters and their parent galaxies of the red cloud (top panel of Fig. 3, $D_n4000_{\rm red,neon} = 1.72 \pm 0.01$). It is reasonable to assume the D_n4000 spectral index to be a tracer of the stellar ages even in the presence of an obscured AGN. The AGN host colours and D_n4000 values are not expected to be significantly affected by the AGN light (Wang et al. 2017; Pierce et al. 2010). We recall here that the AGN is not the dominant mechanism in our sources, and each optical spectrum has been visually inspected in the process of redshift determination when we assign also a special flag for Type 1 AGN (not included as explained in Sect. 1). Under this assumption blue and green [NeV] emitters have a younger stellar population compared to galaxies of the blue cloud and green valley.

In Sect. 3.1, we found that the blue [NeV] emitters to be more massive than their parent galaxies while the red [NeV] emitters are slightly less massive (but within the errors). The blue and red [NeV] emitters thus have very different stellar mass distributions. Given the correlation between the D_n4000 index and stellar mass for galaxies within the blue cloud (Haines et al. 2017) or on the red sequence (Siudek et al. 2017), it is important to verify whether the reported differences in the D_n4000 values between the [NeV] emitters and their parent galaxies (in the green valley and in the blue cloud) remain statistically significant assuming a similar stellar mass distribution. Therefore we build new catalogues using a different approach so as to have [NeV] emitters and their parent galaxies of the three colour-selected classes with equivalent distributions in both stellar mass and redshift. However, being the blue [NeV] emitters more massive than their parent sample, they would have a lower D_n4000 when lowering the stellar mass distribution; this trend is expected based on the interplay observed between this index and stellar masses over the past 8 Gyr (Kauffmann et al. 2003c; Vergani et al. 2008; Haines et al. 2017). This property would enhance the observed behaviour. Nevertheless, for the sake of consistency we have selected all [NeV] emitters from the flux-limited sample of galaxies in the red sequence, green valley, and blue cloud. From these, we create redshift and stellar mass matched catalogues of [NeV] emitters as well as of non-[NeV] emitters, following the same procedure outlined in Sect. 2.3. In other words, instead of using all green galaxies as reference, building stellar mass−redshift matching samples, and then extracting the [NeV] emitters from these, we have used all [NeV] emitters and parent samples,

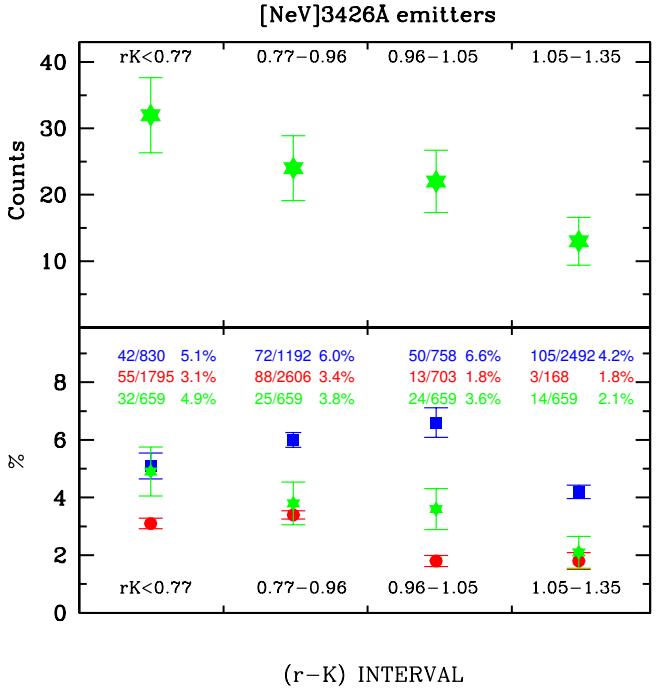

Fig. 4. *Top*: absolute numbers of [NeV] emitters within the green valley, computed in four equally-populated intervals of the $(r-K)$ colour. Error bars represent the Poissonian uncertainty. *Bottom*: fractions of [NeV] emitters among the red sequence (red circles), green valley (green stars) and blue cloud (blue squares) galaxy populations. Error bars on the blue and red points are computed using the resampling technique. The fraction of [NeV] emitters in the green valley is preferentially higher in galaxies with bluer $(r-K)$ colours.

and then built the matched samples. We find that our conclusions are unaffected by the possible caveat induced by the different stellar mass distribution of [NeV] emitters. Using these new catalogs, the 4000 Å Balmer break median value is lower for blue [NeV] emitters ($D_n4000_{\rm blue,neon} = 1.22 \pm 0.01$, compared with 1.30 we obtained before) as well as for blue galaxies ($D_n4000_{\rm blue} = 1.29 \pm 0.01$ compared with previous value of 1.34), but the difference between them remains significant at more than 3σ level. Equally significant remains the difference in D_n4000 reported for the green objects, while the D_n4000 values of the red sub-samples remain the same. We can safely conclude that the [NeV] emitters of the green valley and those of the blue cloud have a younger underlying stellar population compared to their parent population when using as tracer the 4000 Å Balmer break.

3.3. Fractional abundances of [NeV] emitters

Schawinski et al. (2014), and references therein, claim that there are two populations of galaxies in the green valley, with different global properties and pathways to the red sequence. Using the VIPERS Multi-Lambda Survey, Moutard et al. (2016b) identify as fast-quenching objects those galaxies in the NUVrK diagram with very blue colours $(r-K) < 0.76$. These fast quenching objects are mostly characterised by young stellar populations and feed the low-mass part of the red sequence. In summary, the majority of the quiescent population has as progenitors evolved massive star forming galaxies with $(r-K) > 0.76$, while a small fraction is the result of a fast quenching process, involving AGN activity, occurring for blue and low mass objects.

To investigate the impact of AGNs in quenching the star formation activity in galaxies, we show in Fig. 4 the relative frequency of [NeV] emitters as a function of their $(r-K)$ colour. In the top panel we show the number of green [NeV] emitters in four $(r-K)$ colour bins (indicated in the figure). The four bins have been chosen so that they contain equal numbers of green galaxies from the matched samples. In the bottom panel, we show instead the fraction of [NeV] emitters in the matched samples of the three galaxy populations. The total number of [NeV] emitters in each colour bin is annotated along with the total number of objects, and their fractions for the blue, red, and green galaxies, respectively.

The top panel of Fig. 4 shows that the absolute number of the [NeV]λ3426 emitters in the green valley becomes progressively larger towards bluer $(r-K)$ colours, increasing by about a factor of 2.3 from the reddest bin to the bluest bin. In the bottom panel the fraction of green [NeV] emitters compared to the parent samples goes from 2.1% ± 0.5% in the reddest $(r-K)$ bin up to 4.9% ± 0.4% in the bluest region of the green valley. The same increase in the fraction of [NeV] emitters in the green valley towards bluer $(r-K)$ colours is observed at lowering 4000 Balmer break values with a high confidence level, ranging from 2.1% ± 0.2% for $D_n4000 > 1.74$ up to 6.2% ± 0.2% in the region of the green valley with $D_n4000 < 1.48$. No clear trend is observed in the other two classes of the blue and red galaxies which have on average a fraction of $5.5\% \pm 0.2\%$ and $2.5\% \pm 0.1\%$ [NeV] emitters, respectively.

The increasing fraction of galaxies hosting AGNs at larger stellar mass is discussed at length in the literature (Kauffmann et al. 2003a). Similar trends with the quenching efficiency and stellar mass have been observed for $\log(\mathcal{M}_*/\mathcal{M}_\odot) > 10$ galaxies (Kaviraj et al. 2007). Figure 5 shows the percentage of the [NeV] emitters as a function of stellar mass for the green, red, and blue galaxies. The stellar mass intervals indicated in the figure represent quartiles of the stellar mass distribution in the green valley. The total number of the [NeV] emitters in each stellar mass bin and class is annotated above the corresponding histogram, along with the total number of objects in that bin. The relative abundances of [NeV] emitters with respect to their parent population in the blue cloud and red sequence show opposite trends with stellar mass. The [NeV] fraction in the blue population increases progressively with stellar mass, ranging from $3.5\% \pm 0.1\%$ in the low-stellar mass tail up to $7.5\% \pm 0.2\%$ in the most massive bin. On the contrary, the fraction of [NeV] emitters in the red sequence is $\sim 3.4\% \pm 0.1\%$ in the lowest stellar mass bin and diminishes in the high-mass bin (down to $2.5\% \pm 0.1\%$). The green [NeV] emitters are at the level of $3.6\% \pm 0.8\%$ showing no statistical dependence on stellar mass.

The bottom panel of Fig. 5 relates the luminosity of the [NeV]λ3426 line to stellar mass. The lines show the least squares fit to the data (solid, dashed, and dotted lines for the blue, green, and red [NeV] emitters, respectively). The blue squares represent [NeV] emitters from the blue cloud; the green diamonds those of the green valley, and the red circles those in the red sequence. We observe equal increases of the [NeV]λ3426 line luminosity with increasing stellar mass for the three colour-selected classes of [NeV] emitters. The slope of the relation is $\beta = 0.46 \pm 0.02$ in all three cases, while the intercepts decrease with redder colours, $\alpha_{\rm blue} = 35.99 \pm 0.03$, $\alpha_{\rm green} = 35.93 \pm 0.04$, and $\alpha_{\rm red} = 35.66 \pm 0.03$. This similar dependence among the three classes of [NeV] emitters supports the intrinsic nature of the (opposite) trends in the abundance of blue or red [NeV] emitters with stellar mass (Fig. 5, top panel). If it is simply the bulge mass defining whether the galaxy is an [NeV] emitter, we would

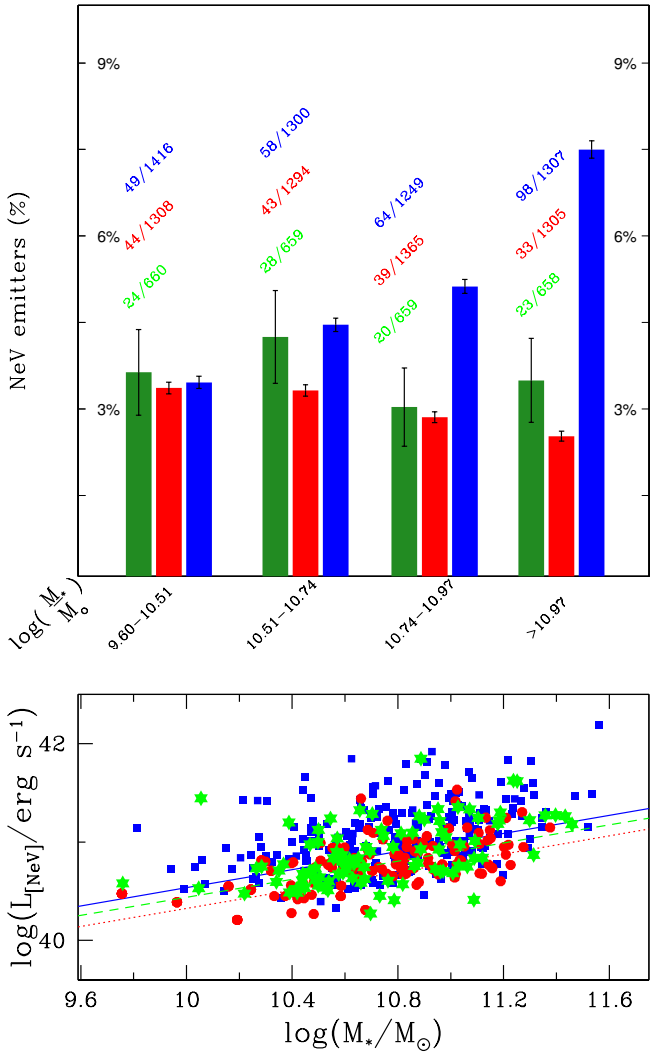

Fig. 5. *Top*: percentage of [NeV] emitters as a function of stellar mass for the green, red and blue galaxies. The fraction of the [NeV] emitters increases with mass in the blue cloud and decreases in the red sequence, but no statistical trend is observed in the green valley. *Bottom*: luminosities in the [NeV] line as a function of stellar mass. Symbols as in Fig. 4. Solid, dashed, and dotted lines show the least squares fits to the blue, green, and red [NeV] emitters, respectively. An increasing [NeV]λ3426 line luminosity is observed at larger stellar masses.

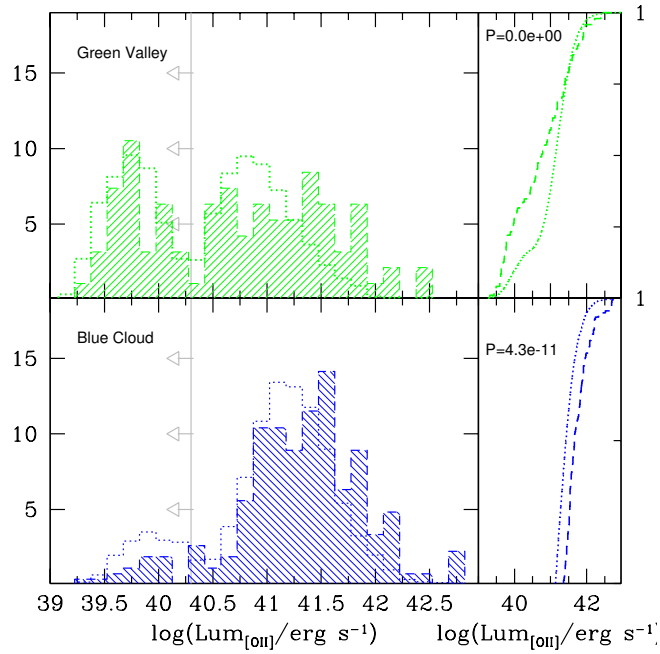

Fig. 6. Distribution of the [NeV] (*top*) and [OII] (*bottom*) luminosities (in erg s^{-1}) of the [NeV] emitters and their parent populations plotted in logarithmic scale. Symbols and numbers are as in Figs. 4 and 5, respectively. The *t*-student test and Kolmogorov–Smirnov test consider as extremely statistically significant, the difference between the luminosity (in the [OII] line) distributions of [NeV] emitters (dashed curve) and their parent samples (dotted curve). The vertical lines and arrows represent the luminosities where the 3σ upper limits enter in the computation. The difference between [NeV] emitters and their parent galaxies remains statistically significant even if only the detections are considered.

see more [NeV] emitters in the red sequence than in the blue galaxies. Also, the bulge mass will be increasing with stellar mass within the red sequence, while the fraction of [NeV] emitters declines.

Other findings support the physical nature of this behaviour. As found in Gilli et al. (2010), the [NeV] luminosity correlates with the X-ray luminosity that itself correlates with the bolometric luminosity, even if a spread of ∼1 dex in luminosities is observed at ±1σ. Thus we can reasonably assume that the [NeV] luminosity is a good indicator of the AGN bolometric luminosity. If we also assume that the Eddington ratio distribution does not change as a function of AGN luminosity, we should detect a larger fraction of [NeV] emitters in bulge-dominated systems. In Fig. 5 (top panel) we observe in blue [NeV] emitters the same trend observed in the local Universe by Bluck et al. (2014) where a larger bulge fraction has been detected in larger stellar mass galaxies over a large range of stellar masses. Furthermore, (Bruce et al. 2016; and references therein) find that lower mass log($\mathcal{M}_*/\mathcal{M}_\odot$) < 10.60 AGN hosts have a higher mean bulge fraction than the control sample. This study has been conducted on a sample of moderate luminosity X-ray selected AGN host galaxies at z = [0.5−3.0], a population rather similar to our red population. The decrease of [NeV] emitters over the red galaxies with the stellar mass may reflect this property.

3.4. [OII] Luminosity

In Fig. 6 we present the total (left) and cumulative (right) distributions of the [OII] line luminosity for the [NeV] emitters (filled, dashed curve) and for their parent samples (dotted curve) in the green valley (top panel) and in the blue cloud (bottom panel). Both detected and upper limits to the [OII] line luminosity are considered in this comparison. The vertical line in the left panels indicates the luminosity at which we start dealing with 3σ upper limits instead of detections. The fraction of upper limits in the various samples are as follows: 8.9% blue [NeV] emitters and 16.5% their parent galaxies; 33.7% green [NeV] emitters and 44.2% their parent galaxies; 57.7% red [NeV] emitters and 62% their parent galaxies. As nearly two third of the red samples are composed by non detections for the [OII] line, from this point on we performed the analysis for the blue and green galaxies only.

For both samples, the [NeV] emitters show higher [OII] luminosities than their corresponding parent sample. We find such differences to be statistically significant when applying both the Student's *t*-test (which gives a confidence level of more than 99.9% for the two distributions to be different), and the Kolmogorov–Smirnov test (which shows a nearly null

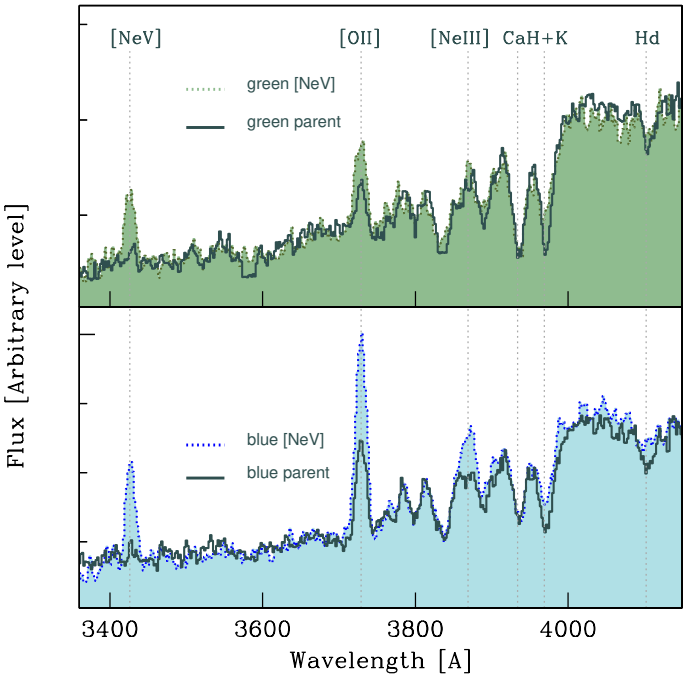

Fig. 7. Stacked rest-frame spectra of [NeV] emitters in the green valley (green dotted line in the *top panel*) and blue cloud (blue dotted line in the *bottom panel*), and of their parent samples (grey solid lines curves in both panels). The parent samples contain all galaxies selected as being independent of the presence of the [NeV] line.

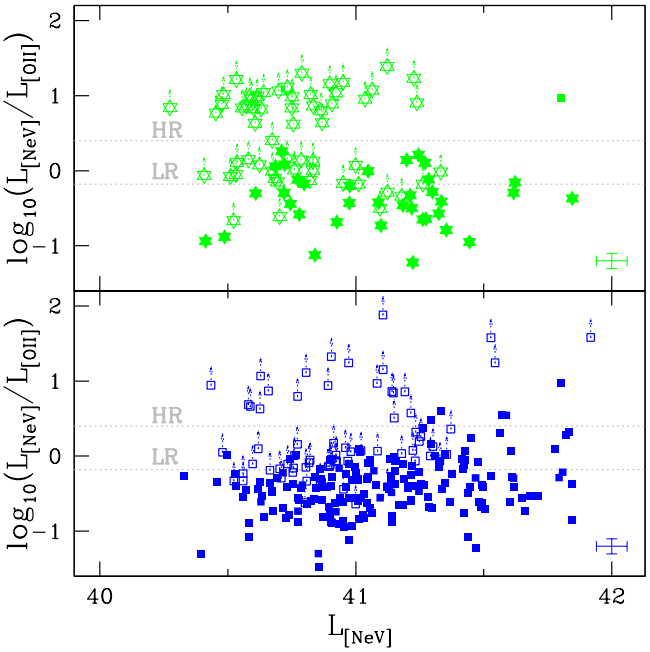

Fig. 8. [NeV]-over-[OII] emission line ratios as a function of [NeV] luminosity for [NeV] emitters in the green valley (*top*) and blue cloud (*bottom*). Solid symbols are [OII] detected sources. Open symbols and arrows represent 3σ upper limits for [OII] non-detections. The typical error bars associated with these quantities are plotted in the bottom right corner of the two panels. The horizontal lines show the separation of each class into three equally populated regions. The combined spectra of galaxies with extreme ratios (HR and LR) are plotted in Fig. 9.

probability for the two samples to be drawn from the same parent population). Such differences remain statistically significant if only detections are considered. We can safely state that the [NeV] emitters show higher [OII] luminosities than their parent galaxies in both the blue cloud and the green valley. This difference can be attributed to the AGN contribution to the [OII] line.

3.5. Spectral properties

Using stacked spectra we can investigate whether the [NeV]λ3426 emitters show distinct features that are peculiar for this population of objects. In other words, our goal is to explore whether the presence of the [NeV] emission line, a proxy of nuclear activity, has an influence on the spectral properties of the host galaxy.

To address this question, we compared the stacked spectra of [NeV] emitters in the green valley and in the blue cloud. They have been produced by shifting each spectrum to the rest frame, and normalising the rest-frame spectrum in the wavelength range λ = 3500−3700 Å before median combining. Spectra with technical problems around the regions of the [NeV] and [OII] lines have been removed from the stacking analysis. We compared the spectral characteristics of these [NeV] emitters with spectra collected from the stellar mass−redshift matched catalogues of the green and blue galaxies independent of the presence, or not, of the [NeV]λ3426 line in their spectra. Those spectra with clean regions around 3426 Å and 3727 Å are combined following the methodology as described above.

We observed weaker [OII] emission lines produced by the star formation process in the composite spectrum of 70 [NeV] emitters from the green valley compared to that of 220 [NeV] emitters of the blue cloud (Fig. 7). The EW[OII] is 1.5−2 times larger in the [NeV] emitters (in the blue and green catalogues) when compared to the stacked spectra from their respective parent samples (1802 green galaxies and 4105 blue galaxies), consistent with a contribution to the [OII] emission from the AGN. The [NeV] emission line is barely detected in the stacked spectra from either the green valley or the blue cloud parent samples, making this line – on average – a very faint spectral feature to reveal in galaxies.

After a visual inspection of each spectrum used in the stack, we identify two classes of galaxies: those galaxies with the [NeV] line only ([NeV] pure emitters), and those with both [NeV] and [OII] lines (combined emitters). Thus we separate the galaxies using a quantitative criterion based on the [NeV]-over-[OII] luminosity ratio. We separated the [NeV] emitters of the green valley into three equally populated intervals based on the [NeV]/[OII] luminosity ratio (0.1−0.7), (0.8−2.5), and (2.6−24), including [OII] upper limits. We defined them as low ratio (LR), intermediate, and high ratio (HR) emitters. The same separation has been adopted to separate the [NeV] emitters in the blue cloud. We end up with 24 (HR) and 22 (LR) green [NeV] emitters, and 28 (HR) and 129 (LR) blue [NeV] emitters. The typical [NeV]/[OII] luminosity ratio in AGN is 0.67 (Netzer 1990), consistent with the upper end of the LR class. Thus, the lower ratios in this class can be easily explained by an additional contribution to the [OII] luminosity from star formation activity.

Figure 8 shows the luminosity of the [NeV] line and that of its ratio over the [OII] line luminosity for the green and blue [NeV] emitters in logarithmic scale, in the top and bottom panels, respectively. The typical error bar associated with these quantities is plotted in the bottom right corner of each panel.

Figure 9 shows the stacked spectra of the two extreme populations of LR (panel a) and HR [NeV] line emitters (panel b) from the green valley (green solid line) and the blue cloud (blue

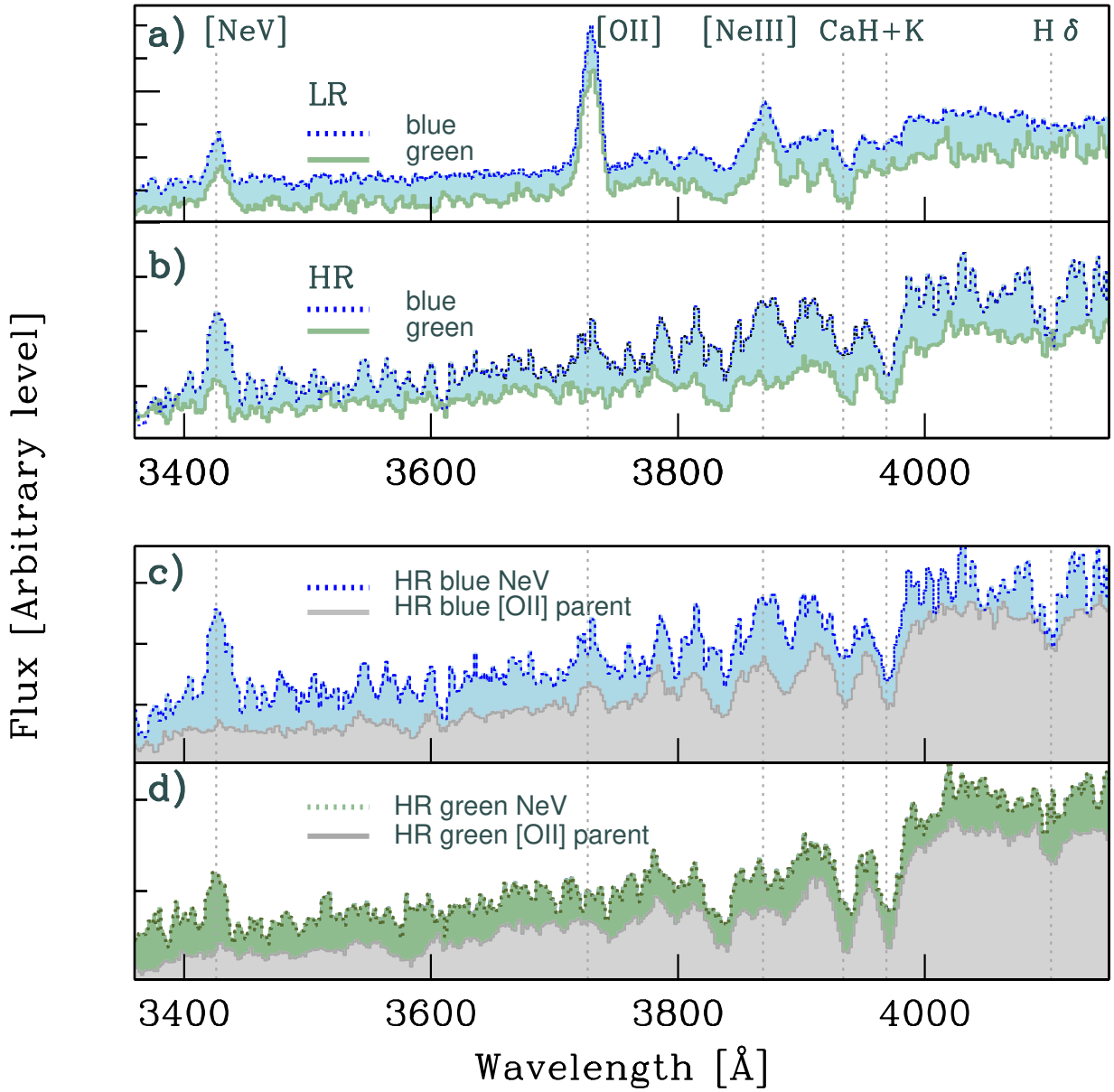

Fig. 9. Combined spectra of [NeV] emitters with LR (*panel a*) and HR (*panel b*) from the green valley (green solid line) and the blue cloud (blue dotted line). *Panel c*: stacked spectrum of the HR blue [NeV] emitters (blue dotted line) overlapped to the combined spectrum of the blue galaxies (grey solid line) with equivalent distributions of stellar mass, redshift, and [OII] luminosity. Strong Balmer absorption lines (Hδ, Hϵ blended in CaII Hλ3968) are features observed in HR blue emitters only. *Panel d*: same as in panel c for the green galaxies and HR green [NeV] emitters. We have applied an offset to the spectra for clarity.

dotted line). The features we observe can be summarised as follows:

- The stacked spectra of green and blue [NeV] emitters with low [OII]/[NeV] ratios (LR) show similar spectral features, typical of star forming galaxies and AGN, with consistent line ratios (Fig. 9a).
- The stacked spectra of the HR blue and green [NeV] emitters instead show some clear differences (Fig. 9b). The former shows a significant Hδ absorption line (in other words, EW(Hδ) ~7.2 Å) which is absent in the HR green [NeV] emitters, and the CaII Hλ3968+Hϵ is deeper than the CaII Kλ3934 Å absorption line (in other words, with a ratio of 0.79). The HR green [NeV] emitters exhibit properties typically associated with an old stellar population.

We note that the absorption contribution of Hδ measurements may be under-estimated, due to the possible emission component of Balmer lines not being evaluated in this study.

To investigate whether the simultaneous presence of strong Balmer absorption lines and very faint [OII] lines in the stacked spectrum of HR blue emitters is simply due to the fact that we have imposed a low flux level for the [OII] line for these objects (in other words [OII] $< \frac{1}{2.6} \times$ [NeV]), or is instead connected with (or induced by) the presence of the [NeV] line, we have built a set of composite spectra of galaxies drawn from the green valley and the blue cloud independent of the [NeV] line detection, but satisfying the condition that their [OII] luminosity distribution is statistically consistent with that of the HR [NeV] emitters.

Thanks to the large sample size of VIPERS, we can afford to build a parent sample with these characteristics that is ten times

larger than the [NeV] counterparts. These parent galaxies (from here on, the [OII] parent population) have equivalent distributions of the stellar mass, redshift, and [OII] luminosity of the HR emitters. These matching catalogues are built separately for the green valley and the blue cloud populations based on their own properties. We produce stacked spectra for this parent population following the same prescription described above.

In panel c of Fig. 9 the blue dotted line shows the stacked spectrum of the HR blue [NeV] emitters (same as panel b) while the grey solid line shows the stacked spectrum of the blue [OII] parent population. We can see that the [OII] parent population does not show the inverted CaII H&K ratio, and the Hδ absorption line is less important (EW(Hδ) = 2.9 ± 0.4 Å) compared to previous case. This difference suggests that the peculiar spectral properties seen in the blue HR [NeV] stacked spectrum are associated with the presence of the [NeV] line and thus with the AGN activity.

In panel d of Fig. 9 we show the same comparison for the objects in the green valley: the stacked spectrum of the HR green [NeV] emitters (green dotted line, same as panel b) is overlaid upon the combined spectrum of the green [OII] parent population (grey solid line). The two spectra do not show any significant differences besides the presence of the [NeV] line. We can conclude that in the green valley the presence of the [NeV] line, and thus of an AGN, is not mirrored by different properties in the host spectrum.

The deep Hδ Balmer absorption feature is observed in galaxies when early-type stars (A-stars) dominate the main-sequence contribution near the epoch of the observation. The Ca H/K line ratio is constant in stars later than F02, while it increases dramatically for earlier type stars as the CaII lines weaken and Hϵ strengthens (Rose 1984). In addition to these spectral properties, we also observe a weak [OII] line in the stacked spectrum of HR blue [NeV] emitters. This line is emitted in HII regions around O and B stars, and it is an indicator of recent star formation (with a lifetime of 10^7 yr). Since the AGN can also contribute to [OII] emission, its weakness implies a low, or even absent, star formation activity in these galaxies. These properties describe a class of galaxies in which there has been a very recent episode of star formation (with a burst dated back by 200–300 Myr), responsible for the inverted Ca H/K line ratio, which has now (almost) stopped (hence the extremely low [OII] emission).

We thus simultaneously observe an AGN indicator (in other words the [NeV] line) and recently stopped star-forming activity (in other words no [OII] emission, inverted CaII H/K ratios, and deep Hδ in absorption) in the blue cloud sources selected on the basis of a high [NeV] /[OII] ratio luminosity ratio. Whether and how the two observables are linked is not clear. We can however affirm that these sources, under certain conditions that are not linked to the stellar mass, the redshift, or the [OII] luminosity, have a short quenching time, in other words, shorter than typical crossing time $\tau < 1$ Gyr, as we cannot see their presence in the green valley. Of course we cannot exclude the possibility that by the time these sources enter and cross the green valley, they no longer have any significant [NeV] line, thus they are not identified as [NeV] emitters. This would imply that we caught these objects during a short phase across their path to the red sequence.

3.6. Possible biases due to the AGN

A contamination by the AGN light may make the observed UV-NIR continuum bluer (Hickox et al. 2009), mimicking the presence of young stars and thus affect the source classification and some of the results presented in previous sections. However, in general, the integrated optical and UV-optical colours are not strongly affected by the AGN with the exception of rare cases (<10%) where the AGN is very luminous, and unobscured (Pierce et al. 2010). Only in those cases, such a contribution can be up to 25%, depending on the observed wavelength, and yield a misclassification of a red galaxy as a green or blue one (e.g. Pierce et al. 2010). As described in Sect. 2.2, objects in regions near the borders of the three colour-selected classes have been omitted to mitigate an artificial migration of objects from one class to another in the NUVrK diagram caused by a colour alteration (of any origin).

Regarding the trends observed in the [NeV] emitters compared to their parent samples, we report below several arguments that disfavour the hypothesis that they might be due to the presence of the AGN instead of being intrinsic to the host. First, in this work, the [NeV] emitters do not host a luminous unobscured AGN by selection, thus the AGN contribution to the optical light is not expected to change the colours significantly.

In addition, the colours considered in quantifying the AGN contribution in the literature are usually based on bluer-bands, such as $u - r$ (Hickox et al. 2009), NUV$-r$ (Pierce et al. 2010), or U−B (Pierce et al. 2010), while we used a redder colour ($r-K$) that is less affected by this blueing effect because the continuum of the AGN becomes red at >1 μm (Elvis et al. 1994). Finally, the trend reported on the population of [NeV] emitters from the green valley (in other words, larger fraction at bluer $r-K$) is confirmed not only using photometric broad-bands but also when we analyse the spectral D_n4000 index. The latter is less affected by the AGN continuum as it is based on a narrow spectral portion around 4000 Å.

As a final check, we also estimated the AGN contribution to the spectral energy distribution (SED) in the [NeV] emitters and in their parent samples using the spectral energy modelling code CIGALE[1] (Noll et al. 2009). We modelled their optical-NIR SEDs (8 broad-bands from u to K) with the stellar population synthesis models by Bruzual & Charlot (2003) with a delayed star formation history after a burst. The effect of dust was treated assuming the Charlot & Fall (2000) attenuation law, and the dust properties of Draine & Li (2007). The AGN component, including the accretion disk and the dusty torus emission, was modelled after Fritz et al. (2006). The fits yield a median fractional contribution of the AGN component to the bolometric luminosity in [NeV] emitters of 10% in all three classes, and of 5%, 14%, and 10% in the parent red, green and blue galaxies, respectively, with typical errors of the order of ±4%. We thus find no significant difference in the AGN contribution between [NeV] emitters and their parent samples. In conclusion, we have shown that the influence of the nuclear activity should not be artificially altering the properties of the host galaxy in [NeV] emitters, and thus it does not affect our results.

3.7. [NeV] emitters vs. other AGN selection techniques

In Sect. 1, we described other AGN selection techniques, for example, those based on the X-ray luminosity, mid-IR colours, the MEx diagram, or optical emission line ratios. These techniques yield AGN samples with different levels of completeness and purity, and these depend on the depth of the data. In this work, we have adopted a less common technique for several reasons: our selection based on the detection of the [NeV] line yields a highly reliable AGN sample (Gilli et al. 2010; Mignoli et al. 2013), and it can be applied to the full VIPERS

[1] Code Investigation GALaxy Emission, http://cigale.lam.fr/

Table 1. [NeV] emitters vs. other AGN selection techniques.

Sample	N	N in W1	N X-ray AGN (%)	N MIR-AGN (%)	N MEx AGN (%)	N BBPT AGN (%)
Blue [NeV]	269	200	11 (5.5 ± 1.7)	9 (4.5 ± 1.5)	24 (9 ± 2)	21 (8 ± 2)
Blue parent	5272	3552	47 (1.3 ± 0.2)	33 (0.9 ± 0.2)	112 (2.0 ± 0.2)	67 (1.3 ± 0.2)
Green [NeV]	95	62	1 (1.6 ± 1.6)	1 (1.6 ± 1.6)	4 (4 ± 2)	4 (4 ± 2)
Green parent	2636	1708	13 (0.8 ± 0.2)	7 (0.4 ± 0.2)	12 (0.5 ± 0.1)	10 (0.4 ± 0.1)
Red [NeV]	157	120	1 (0.8 ± 0.8)	0 (0.0)	0 (0.0)	0 (0.0)
Red parent	5272	3501	11 (0.3 ± 0.1)	5 (0.14 ± 0.06)	0 (0.0)	0 (0.0)

Notes. X-ray AGN: X-ray detected sources with X-ray luminosities greater than 10^{42} ergs s^{-1} or with $N_{\rm H} \geq 10^{22}$ cm^{-2}. MIR-AGN: sources with 5σ detections at 3.6 μm and 4.5 μm and with S(4.5 μm)/S(3.6 μm) $\geq$ 1.27 (Stern et al. 2012). MEx AGN: sources with more than 3σ Hβ and [OIII] equivalent widths and EW([OIII])/EW(Hβ) ratios satisfying the MEx AGN selection criterion defined in Juneau et al. (2011). BBPT AGN: sources with more than 3σ Hβ, [OII], and [OIII] equivalent widths and EW([OIII])/EW(Hβ) and EW([OII])/EW(Hβ) ratios satisfying the blue BPT criterion defined in Lamareille (2010).

sample. In addition, numerous previous works have already investigated the incidence of AGN identified by these techniques in the green valley or in transitioning galaxies (e.g. Yan et al. 2006; Schawinski et al. 2010, 2014). While they all find higher fractions of AGN in the green valley, there is no clear evidence of negative feedback from these AGN. Since different selection techniques yield AGN samples that do not fully overlap and might favour different evolutionary phases (Hickox et al. 2009), it is interesting to investigate and compare results obtained with different AGN samples.

We have conducted this analysis using the ancillary data available in the VIPERS fields to quantify the fraction of [NeV] emitters that would be selected as AGN by the most common selection techniques. In particular, we have used the X-ray data from the XXL survey (Pierre et al. 2016), the *Spitzer* data from the SWIRE survey (Lonsdale et al. 2004), the WISE data from the AllWISE data (Wright et al. 2010), as well as spectral measurements from VIPERS itself, but requiring the detection of multiple emission lines, i.e. Hβ, [OIII], and/or [OII] (MEx and blue BPT diagrams, Juneau et al. 2011; Lamareille 2010). Each of these criteria can only be applied to sub-sets of the VIPERS sample, because the X-ray and *Spitzer* coverage is limited to a fraction of the W1 field, and because the lines necessary to apply the MEx or blue-BPT diagnostic diagrams are only available for objects up to $z \sim 0.89$. The numbers and fractions of [NeV] emitters selected by these techniques are listed in Table 1. Overall, we find that only a small fraction, i.e. <10%, of [NeV] emitters are selected by these techniques. In all cases, the fraction of selected AGN is higher among the [NeV] emitters than in their parent samples: by a factor of five in the blue and green samples and a factor of two in the red one. This analysis also shows that the AGN contamination in the parent samples is negligible, i.e. $\leq$2%. We note that this is true even if [NeV] emitters are present in the parent samples. None of [NeV] emitters occupy the lineRs region both using the few measured [OIII]5007 & Hβ lines or upper limits computed as five times the errors on the EW for the undetected sources.

This comparison indicates that the AGN selected by the strength of the [NeV] line are not commonly represented in shallow X-ray, mid-IR, MEx, or BPT selected samples, and any peculiarity found in this class might be linked to what makes this line detectable.

It is interesting to note that 12 out of the 13 X-ray detected [NeV] emitters are obscured and their X-ray-over-[NeV] luminosity ratios are consistent with those measured in other X-ray detected [NeV] emitter samples (Gilli et al. 2010), thus confirming that [NeV] sources are mostly obscured AGN. However, we note that the numbers of [NeV] emitters detected in the X-rays, or with hot dust signatures in their mid-IR SEDs, are too low to draw any significant conclusion on their properties based on these data (see also Gilli et al. 2010; Mignoli et al. 2013).

In contrast to previous studies based on the classical AGN selection techniques, we do not find an enhancement of AGN in the transition galaxies, but a decreasing fraction from 5.2%, to 3.6%, and 3.0% going from the blue cloud, to the green valley, and red sequence galaxies. We also find a different trend with respect to the stellar mass; with the incidence of AGN increasing towards higher masses in the blue cloud, but decreasing with mass in the red sequence. Previous studies based on X-ray selected AGN find an increase in the AGN fraction with stellar mass in the red and green samples and no variation among blue galaxies (Wang et al. 2017).

4. Discussion

In the past two decades observational studies at various wavebands have supported the idea of a stochastic fueling of AGN in galaxies, with no evidence for AGN feedback on the star formation activity of the host galaxies. However various observational findings and theoretical studies provide also an alternative picture supporting a close connection between AGN activity and the host galaxies (e.g. Boyle & Terlevich 1998; Silverman et al. 2008; Aird et al. 2010; Le Fèvre et al. 2017), although this impact on galaxy formation and evolution is not yet well understood (Best et al. 2006; Croton et al. 2006; Nesvadba et al. 2008; Smolčić 2009).

In this investigation we present a number of observational facts pointing at differences between active and inactive galaxies supporting the AGN feedback scenario. In this work the nuclear activity is probed by the high-ionisation [NeV]λ3426 emission line and [NeV] emitters with their parent samples are properly selected according to their stellar mass, redshift, and NUVrK colour distributions. Broad-line (Type 1) AGNs have been excluded to focus on galaxies with the stellar light not contaminated by the continuum light from the AGNs.

We find that stellar ages and the [OII] luminosities of the [NeV] emitters appear to be statistically different from the corresponding parent galaxies once properly matched in redshift and stellar mass. In particular, [NeV] emitters are hosted by galaxies with, on average, younger stellar populations (lower D_n4000 values) and higher SFRs (larger [OII] luminosities) than their parent population, if we assume that the [OII] luminosity is a direct probe of the star formation activity in these galaxies.

Stellar ages and SFRs are consistent in active and inactive galaxies when AGNs are selected independently by the host colours, or the morphological aspect. Instead, differences begin to be observed when the samples are carefully selected, though they might be at lower significance level, due to the reduced statistic (Azadi et al. 2017; and references therein). Consistent with previous results we find a larger fraction of green galaxies hosting AGN activity at progressively bluer ($r-K$) colours. This property is in agreement with results reporting an increasing incidence of AGN activity in younger systems, from an X-ray selected sample in the COSMOS field up to $z \sim 1$ by Silverman et al. (2009). These different properties testify to an intimate correlation between the AGN activity and the mechanisms that regulate star formation in the host galaxy.

In addition to the different stellar ages and SFRs, we observe a dependence of AGN fraction on the location of the host in the NUVrK colour diagram; a trend which is mass-dependent. We find a slightly higher fraction of [NeV] emitters among blue cloud galaxies than in the green valley and red sequence. However, such a difference is mass-dependent as it is not observed for galaxies with stellar masses $<3\times10^{10}\,\mathcal{M}_{\odot}$ and it is enhanced at higher masses, i.e. $>9\times10^{10}\,\mathcal{M}_{\odot}$. One possible explanation is that the AGN affects more significantly its host galaxy or viceversa when the host galaxy, and thus the accreting BH, are more massive. The nuclear activity is also more common in progressively massive blue galaxies. The trend with stellar mass has been already observed at different redshifts for different types of AGNs (Kauffmann et al. 2003a; Best et al. 2005; Silverman et al. 2009). Local AGNs selected from the Sloan Digital Sky Survey and visually classified by Schawinski et al. (2010) are found preferentially in massive late-type galaxies with $\log(\mathcal{M}_{*}/\mathcal{M}_{\odot})\sim11$, and moderate-mass early-type systems with $\log(\mathcal{M}_{*}/\mathcal{M}_{\odot})\sim10$, in agreement with our results. This is coherent with Schawinski et al. (2010)'s proposal that black holes have different properties when hosted in either early and red, or late and blue type galaxies.

Conventional line diagnostics can misidentify AGN in composite galaxies with strong star formation activity (e.g. Bär et al. 2017 and references therein). Single, high-ionisation line diagnostics are more sensitive to AGN ionisation in the presence of high levels of star formation, e.g. using the [HeII]λ4685 emission line (Bär et al. 2017), or the [NeV]λ3426 emission line (Gilli et al. 2010; Mignoli et al. 2013, including this work). Bär et al. (2017) report that [HeII]-selected AGNs (in other words, not with the standard BTP diagram) are more commonly found in star-forming galaxies in the blue cloud and above the main sequence at the high masses where quenching is expected to play a role, see Haines et al. (2017). In this respect, the results by Schawinski et al. (2010) who locate the majority of local AGN candidates in the green region may be explained by the use of classical diagnostics. It is also true that if these AGNs are located in an "already transiting" region, then the AGN cannot be the reason for initiating the quenching process, as their host galaxies should have already experienced a star formation suppression. In fact the delay time between the star formation quenching and the detection of emission-lines used to select AGN candidates is expected to be larger than the time a galaxy needs to cross the green valley. In conclusion, it is not surprising to find quenching signatures in active galaxies of the blue cloud if the AGN is the reason for such a star formation quenching. This is, in fact, what we find in this analysis.

We have assessed the relative importance of AGN on the star formation activity by comparing the stacked spectra of two classes of galaxies defined based on their [NeV] over [OII] luminosity ratio. This methodology is similar to the ones adopted in the local Universe – with the ratio of the IR fine structure lines by LaMassa et al. (2012), or analogously to the "D" parameter as distance at which a source lies from the locus of star forming galaxies on the BTP diagram by Kauffmann et al. (2003a). Through this approach we identify a sub-set of [NeV] emitters with high [NeV] to [OII] ratios within the blue cloud, that show signs of recent quenching having experienced a burst of star formation activity in their recent past (<200−300 Myr ago, e.g. Wild et al. 2007, 2010). This is supported by spectral signatures typical of very hot, massive stars (Balmer absorption lines and an inversion of the intensities of the K and H calcium lines, due to the presence of a blend of the calcium H line with the Hϵ Balmer line). Their spectra resemble those of post-starburst galaxies. However they would never be included in a spectroscopic search of post-starburst galaxies because of the limit imposed on the nebular emission lines − powered in these galaxies by both SF and AGN activity (see Alatalo et al. 2016; and references therein).

There have been recent claims of a bimodality in the composition of the population of the green valley. This bimodality has been attributed to the different quenching mechanisms (and the characteristic timescales) in action. Moutard et al. (2016b) use a similar NUVrK diagram to identify green valley galaxies within the VIPERS dataset, as a tracer of galaxy evolution and the quenching process. They identify one main quenching channel (over a moderately long timescale 0.5−2 Gyr) between the star-forming and quiescent sequences at $0.2 < z < 1.5$, that is populated by massive, star-forming galaxies with typically red colours, $(r-K) > 0.76$. Interestingly, they also suggest a second path to the red sequence (with faster quenching timescales) that is followed by bluer, low-mass galaxies. Similarly, in the local universe, Schawinski et al. (2014) find a primary quenching channel of late-type galaxies that move to redder colours with a slow quenching timescale according to the exhaustion of their gas supplies, but also identify a minority of transitioning galaxies that requires a rapid transformation of morphology and colour. Our result that bluer galaxies have a higher probability of hosting an AGN, thus a faster quenching time, and that a fraction of them present quenching signatures are in agreement with the general picture emerging from the conclusions of these studies.

This investigation demonstrates that there exists a link between AGN activity and the sustainability of star formation in the hosting galaxies at $0.62 < z < 1.2$. The presence of the mechanism(s) producing the highly ionised [NeV]λ3426 line, under certain conditions, stops the formation of new stars. These conditions may be related to the efficiency of the black hole and/or the physical conditions of the hosting galaxies, but not linked to stellar mass, redshift, or current star formation (as expressed via the [OII] luminosity). To have a completely quenched system, the cold gas reservoir has to be either fully consumed or heated up entirely. In simulations this is achieved almost instantaneously via AGN feedback (Springel et al. 2005), thus feedback might start before a AGN hosting galaxy reaches the green valley, precisely as we observe in the [NeV] emitters in the blue cloud. Considering that our results are based on a complete spectroscopic sample and limited by the [NeV] observability, and that the AGN can be variable and with a relatively short duty cycle, AGN feedback that makes blue galaxies quickly transition to the red sequence may be even more common than previously believed, at least for galaxies within stellar mass and redshifts explored here.

5. Conclusions

Thanks to the large volume probed by the VIMOS Public Extragalactic Redshift Survey, we have been able to select the largest sample of [NeV] emitters at intermediate redshifts ($z = 0.62-1.2$) available so far. We have used this sample to study the properties of the host galaxies with nuclear activity, as probed by the presence of the high-ionisation potential of the [NeV]λ3426 emission line. The sample comprises 529 [NeV] emitters, matched in redshift and stellar mass, and divided into the red sequence, green valley and blue cloud according to their (NUV$-r$) vs. ($r-K$) colours. We have built mass and redshift matched control samples of galaxies using the full VIPERS survey, to compare with the properties of the active sample.

We report on statistically different properties (stellar age, [OII] luminosity, $r-K$ colour) between active and inactive galaxies, and among the active galaxies different characteristics (stellar mass, fractional number) are observed according to their NUVrK colours. In particular, the main results are as follows:

1. Blue [NeV] emitters are significantly more massive than the [NeV] emitters in the red sequence.
2. The [NeV] emitters in the green valley and in the blue cloud have younger underlying stellar populations compared to their parent populations (using the 4000 Å Balmer break as a tracer).
3. The fraction of [NeV] emitters in the green valley increases by about a factor of 2.5 with decreasing ($r-K$) colour. This is not observed for the [NeV] emitters in the blue cloud or in the red sequence.
4. The abundance of the [NeV] emitters with respect to their parent population in the blue cloud and red sequence show opposite trends with the stellar mass. No statistical trend with stellar mass is observed for the number of [NeV] emitters in the green valley.
5. The [NeV] emitters show a higher [OII] luminosity than that of the parent galaxies in both the blue cloud and the green valley, confirming the contribution of the AGN activity to the [OII] emission.
6. Among the blue cloud galaxies, we identify a sub-set of [NeV] emitters with weak or absent [OII] emission (HR class). Their stacked spectra show signs of a recent burst of star formation, and no current star-formation activity similar to post-starburst galaxies. These objects represent galaxies were star-formation has been recently halted and this is likely linked to the presence of the AGN. In the [NeV] emitters in the green valley and red sequence, star formation has already stopped, presumably when they were in the blue cloud, but the AGN continues to be traceable through the high-ionisation [NeV] line. Based on the properties of the blue [NeV] emitters, we claim that the AGN is more common in more massive galaxies and when their star formation is closer to its peak, as suggested by their blue ($r-K$) colours and low D4000 values.

These observational pieces of evidence taken together point towards a link between the AGN activity and the mechanism(s) that regulate the star formation in the host galaxy. We also reveal the existence of a novel class of AGN hosting galaxies among the blue galaxies where the AGN may arguably fast quench the star formation and accelerate the evolution from the blue cloud to the green valley.

Acknowledgements. We acknowledge the crucial contribution of the ESO staff for the management of service observations. In particular, we are deeply grateful to M. Hilker for his constant help and support of this programme. Italian participation to VIPERS has been funded by INAF through PRIN 2008, 2010, and 2014 programmes. LG and BRG acknowledge support from the European Research Council through grant no. 291521. OLF acknowledges support from the European Research Council through grant no. 268107. JAP acknowledges support of the European Research Council through grant no. 67093. WJP and RT acknowledge financial support from the European Research Council through grant no. 202686. AP, KM, and JK have been supported by the National Science Centre (grants UMO-2012/07/B/ST9/04425 and UMO-2013/09/D/ST9/04030). WJP is also grateful for support from the UK Science and Technology Facilities Council through the grant ST/I001204/1. EB, FM and LM acknowledge the support from grants ASI-INAF I/023/12/0 and PRIN MIUR 2010–2011. LM also acknowledges financial support from PRIN INAF 2012. YM acknowledges support from CNRS/INSU (Institut National des Sciences de l'Univers). CM is grateful for support from specific project funding of the Institut Universitaire de France. SDLT and CM acknowledge the support of the OCEVU Labex (ANR-11-LABX-0060) and the A*MIDEX project (ANR-11-IDEX-0001-02) funded by the "Investissements d'Avenir" French government programme managed by the ANR. and the Programme National Galaxies et Cosmologie (PNCG). Research conducted within the scope of the HECOLS International Associated Laboratory, supported in part by the Polish NCN grant DEC-2013/08/M/ST9/00664. Finally, DV acknowledges the help received by M. Sandri in computing coding.

References

Aird, J., Nandra, K., Laird, E. S., et al. 2010, MNRAS, 401, 2531
Akylas, A., & Georgantopoulos, I. 2009, A&A, 500, 999
Alatalo, K., Cales, S. L., Rich, J. A., et al. 2016, ApJS, 224, 38
Alexander, D. M., Bauer, F. E., Brandt, W. N., et al. 2011, ApJ, 738, 44
Appleton, P. N., Fadda, D. T., Marleau, F. R., et al. 2004, ApJS, 154, 147
Azadi, M., Coil, A. L., Aird, J., et al. 2017, ApJ, 835, 27
Baldwin, J. A., Phillips, M. M., & Terlevich, R. 1981, PASP, 93, 5
Balogh, M. L., & Morris, S. L. 2000, MNRAS, 318, 703
Balogh, M. L., Morris, S. L., Yee, H. K. C., Carlberg, R. G., & Ellingson, E. 1999, ApJ, 527, 54
Bär, R. E., Weigel, A. K., Sartori, L. F., et al. 2017, MNRAS, 466, 2879
Barnes, J. E., & Hernquist, L. 1992, ARA&A, 30, 705
Best, P. N., Kauffmann, G., Heckman, T. M., et al. 2005, MNRAS, 362, 25
Best, P. N., Kaiser, C. R., Heckman, T. M., & Kauffmann, G. 2006, MNRAS, 368, L67
Bluck, A. F. L., Mendel, J. T., Ellison, S. L., et al. 2014, MNRAS, 441, 599
Boyle, B. J., & Terlevich, R. J. 1998, MNRAS, 293, L49
Brandt, W. N., & Hasinger, G. 2005, ARA&A, 43, 827
Brightman, M., Nandra, K., Salvato, M., et al. 2014, MNRAS, 443, 1999
Bruce, V. A., Dunlop, J. S., Mortlock, A., et al. 2016, MNRAS, 458, 2391
Bruzual, G., & Charlot, S. 2003, MNRAS, 344, 1000
Buchner, J., Georgakakis, A., Nandra, K., et al. 2015, ApJ, 802, 89
Charlot, S., & Fall, S. M. 2000, ApJ, 539, 718
Comastri, A., Ranalli, P., Iwasawa, K., et al. 2011, A&A, 526, L9
Croton, D. J., Springel, V., White, S. D. M., et al. 2006, MNRAS, 365, 11
Cucciati, O., Davidzon, I., Bolzonella, M., et al. 2017, A&A, 602, A15
Davidzon, I., Bolzonella, M., Coupon, J., et al. 2013, A&A, 558, A23
Davidzon, I., Cucciati, O., Bolzonella, M., et al. 2016, A&A, 586, A23
Davies, R. L., Kewley, L. J., Ho, I.-T., & Dopita, M. A. 2014, MNRAS, 444, 3961
Della Ceca, R., Caccianiga, A., Severgnini, P., et al. 2008, A&A, 487, 119
Draine, B. T., & Li, A. 2007, ApJ, 657, 810
Dressler, A., & Gunn, J. E. 1983, ApJ, 270, 7
Elvis, M., Wilkes, B. J., McDowell, J. C., et al. 1994, ApJS, 95, 1
Feltre, A., Charlot, S., & Gutkin, J. 2016, MNRAS, 456, 3354
Fritz, J., Franceschini, A., & Hatziminaoglou, E. 2006, MNRAS, 366, 767
Garilli, B., Paioro, L., Scodeggio, M., et al. 2012, PASP, 124, 1232
Garilli, B., Guzzo, L., Scodeggio, M., et al. 2014, A&A, 562, A23
Gilli, R., Vignali, C., Mignoli, M., et al. 2010, A&A, 519, A92
Goto, T., Nichol, R. C., Okamura, S., et al. 2003, PASJ, 55, 771
Gunn, J. E., & Gott, J. R. I. 1972, ApJ, 176, 1
Guzzo, L., Scodeggio, M., Garilli, B., et al. 2014, A&A, 566, A108
Haines, C. P., Iovino, A., Krywult, J., et al. 2017, A&A, 605, A4
Hamilton, D. 1985, ApJ, 297, 371
Hickox, R. C., Jones, C., Forman, W. R., et al. 2009, ApJ, 696, 891
Hopkins, P. F., Bundy, K., Hernquist, L., & Ellis, R. S. 2007, ApJ, 659, 976

Ilbert, O., McCracken, H. J., Le Fevre, O., et al. 2013, A&A, 556, A55
Juneau, S., Dickinson, M., Alexander, D. M., & Salim, S. 2011, ApJ, 736, 104
Juneau, S., Bournaud, F., Charlot, S., et al. 2014, ApJ, 788, 88
Kauffmann, G., Heckman, T. M., Tremonti, C., et al. 2003a, MNRAS, 346, 1055
Kauffmann, G., Heckman, T. M., White, S. D. M., et al. 2003b, MNRAS, 341, 33
Kauffmann, G., Heckman, T. M., White, S. D. M., et al. 2003c, MNRAS, 341, 54
Kaviraj, S., Kirkby, L. A., Silk, J., & Sarzi, M. 2007, MNRAS, 382, 960
Kellermann, K. I., Sramek, R., Schmidt, M., Shaffer, D. B., & Green, R. 1989, AJ, 98, 1195
Lamareille, F. 2010, A&A, 509, A53
LaMassa, S. M., Heckman, T. M., Ptak, A., et al. 2012, ApJ, 758, 1
Larson, R. B., Tinsley, B. M., & Caldwell, C. N. 1980, ApJ, 237, 692
Le Fèvre, O., Lemaux, B. C., Nakajima, K., et al. 2017, A&A, submitted [arXiv:1710.10715]
Lonsdale, C., Polletta, M. D. C., Surace, J., et al. 2004, ApJS, 154, 54
Martin, D. C., Wyder, T. K., Schiminovich, D., et al. 2007, ApJS, 173, 342
Mignoli, M., Vignali, C., Gilli, R., et al. 2013, A&A, 556, A29
Morganti, R. 2017, Nat. Astron., 1, 596
Moutard, T., Arnouts, S., Ilbert, O., et al. 2016a, A&A, 590, A102
Moutard, T., Arnouts, S., Ilbert, O., et al. 2016b, A&A, 590, A103
Nesvadba, N. P. H., Lehnert, M. D., De Breuck, C., Gilbert, A. M., & van Breugel, W. 2008, A&A, 491, 407
Netzer, H. 1990, in Active Galactic Nuclei, ed. R. D. Blandford, H. Netzer, L. Woltjer, T. J.-L. Courvoisier, & M. Mayor, 57
Noll, S., Burgarella, D., Giovannoli, E., et al. 2009, A&A, 507, 1793
Pierce, C. M., Lotz, J. M., Salim, S., et al. 2010, MNRAS, 408, 139
Pierre, M., Pacaud, F., Adami, C., et al. 2016, A&A, 592, A1
Rose, J. A. 1984, AJ, 89, 1238
Schawinski, K., Urry, C. M., Virani, S., et al. 2010, ApJ, 711, 284
Schawinski, K., Urry, C. M., Simmons, B. D., et al. 2014, MNRAS, 440, 889
Schmidt, M., Hasinger, G., Gunn, J., et al. 1998, A&A, 329, 495
Scodeggio, M., Franzetti, P., Garilli, B., Le Fèvre, O., & Guzzo, L. 2009, The Messenger, 135, 13
Scodeggio, M., Guzzo, L., Garilli, B., et al. 2018, A&A, 609, A84
Silverman, J. D., Green, P. J., Barkhouse, W. A., et al. 2008, ApJ, 679, 118
Silverman, J. D., Lamareille, F., Maier, C., et al. 2009, ApJ, 696, 396
Siudek, M., Małek, K., Scodeggio, M., et al. 2017, A&A, 597, A107
Smolčić, V. 2009, ApJ, 699, L43
Springel, V., Di Matteo, T., & Hernquist, L. 2005, MNRAS, 361, 776
Stern, D., Assef, R. J., Benford, D. J., et al. 2012, ApJ, 753, 30
Toomre, A., & Toomre, J. 1972, ApJ, 178, 623
Trayford, J. W., Theuns, T., Bower, R. G., et al. 2016, MNRAS, 460, 3925
Vergani, D., Scodeggio, M., Pozzetti, L., et al. 2008, A&A, 487, 89
Vergani, D., Zamorani, G., Lilly, S., et al. 2010, A&A, 509, A42
Vignali, C., Alexander, D. M., Gilli, R., & Pozzi, F. 2010, MNRAS, 404, 48
Wang, T., Elbaz, D., Alexander, D. M., et al. 2017, A&A, 601, A63
Wild, V., Kauffmann, G., Heckman, T., et al. 2007, MNRAS, 381, 543
Wild, V., Heckman, T., & Charlot, S. 2010, MNRAS, 405, 933
Wilkes, B. J., & Elvis, M. 1987, ApJ, 323, 243
Williams, R. J., Quadri, R. F., Franx, M., van Dokkum, P., & Labbé, I. 2009, ApJ, 691, 1879
Wright, E. L., Eisenhardt, P. R. M., Mainzer, A. K., et al. 2010, AJ, 140, 1868
Yan, R., Newman, J. A., Faber, S. M., et al. 2006, ApJ, 648, 281
Yan, R., Ho, L. C., Newman, J. A., et al. 2011, ApJ, 728, 38
Zamfir, S., Sulentic, J. W., & Marziani, P. 2008, MNRAS, 387, 856

[1] INAF – Osservatorio di Astrofisica e Scienza dello Spazio, Via P. Gobetti 93/3, 40129 Bologna, Italy
e-mail: daniela.vergani@inaf.it
[2] INAF – Istituto di Astrofisica Spaziale e Fisica Cosmica Milano, Via E. Bassini 15, 20133 Milano, Italy
[3] Aix-Marseille Université, Jardin du Pharo, 58 bd Charles Livon, 13284 Marseille Cedex 7, France
[4] IRAP, 9 av. du colonel Roche, BP 44346, 31028 Toulouse Cedex 4, France
[5] INAF – Osservatorio Astronomico di Brera, Via Brera 28, 20122 Milano – via E. Bianchi 46, 23807 Merate, Italy
[6] Università degli Studi di Milano, Via G. Celoria 16, 20133 Milano, Italy
[7] Aix–Marseille Univ., CNRS, LAM, Laboratoire d'Astrophysique de Marseille, Marseille, France
[8] INAF – Osservatorio Astrofisico di Torino, 10025 Pino Torinese, Italy
[9] Laboratoire Lagrange, UMR7293, Université de Nice Sophia Antipolis, CNRS, Observatoire de la Côte d'Azur, 06300 Nice, France
[10] Dipartimento di Fisica e Astronomia – Alma Mater Studiorum Università di Bologna, Via P. Gobetti 93/2, 40129 Bologna, Italy
[11] INAF – Osservatorio Astronomico di Trieste, Via G. B. Tiepolo 11, 34143 Trieste, Italy
[12] Institute of Physics, Jan Kochanowski University, ul. Swietokrzyska 15, 25-406 Kielce, Poland
[13] National Centre for Nuclear Research, ul. Hoza 69, 00-681 Warszawa, Poland
[14] INFN, Sezione di Bologna, Viale Berti Pichat 6/2, 40127 Bologna, Italy
[15] Astronomical Observatory of the Jagiellonian University, Orla 171, 30-001 Cracow, Poland
[16] School of Physics and Astronomy, University of St Andrews, St Andrews KY16 9SS, UK
[17] INAF – Istituto di Radioastronomia, Via P. Gobetti 101, 40129 Bologna, Italy
[18] Aix–Marseille Univ., Univ. Toulon, CNRS, CPT, Marseille, France
[19] Dipartimento di Matematica e Fisica, Università degli Studi Roma Tre, Via della Vasca Navale 84, 00146 Roma, Italy
[20] INFN, Sezione di Roma Tre, Via della Vasca Navale 84, 00146 Roma, Italy
[21] INAF – Osservatorio Astronomico di Roma, Via Frascati 33, 00040 Monte Porzio Catone, RM, Italy
[22] Department of Astronomy, University of Geneva, ch. d'Ecogia 16, 1290 Versoix, Switzerland
[23] Department of Astronomy & Physics, Saint Mary's University, 923 Robie Street, Halifax, Nova Scotia B3H 3C3, Canada